Streamwise fences for the reduction of trailing-edge noise in a NACA633018 airfoil

Fiscaletti, D.; Luesutthiviboon, S.; Avallone, F.; Casalino, D.

DOI
10.2514/6.2022-1925

Publication date
2022

Document Version
Final published version

Published in
AIAA SCITECH 2022 Forum

AIAA SciTech Forum
January 3-7, 2022, San Diego, CA & Virtual
AIAA SCITECH 2022 Forum

10.2514/6.2022-1925

Streamwise fences for the reduction of trailing-edge noise in a NACA633018 airfoil

Daniele Fiscaletti*, Salil Luesutthiviboon†, Francesco Avallone‡ and Damiano Casalino§

Streamwise fences for the reduction of the trailing-edge noise are experimentally investigated on a NACA633018 airfoil. Interchangeable trailing-edge inserts with streamwise fences of different spacing and height are tested in an anechoic wind tunnel. Far-field trailing-edge noise was measured by an array of microphone and the airfoil drag was calculated from the wake profiles acquired by a wake rake. The transversal spacing between the fences has a much stronger impact on noise reduction than the fences height. A maximum noise reduction of 5-6 dB is obtained from fences having a spacing of 2 mm, and it is achieved in the range of Strouhal numbers based on the chord of 15-40, equivalent to frequencies 1-3 kHz. When increasing the spacing between the fences from 2 mm to 4 mm, a different aeroacoustic behaviour is observed, with a lower noise reduction at high frequencies, and a higher noise reduction and low frequencies. Increasing the angle of attack from $\alpha = 0°$ to $\alpha = 6°$ does not lead to any significant deterioration of the noise reduction performance. From a wake survey, the coefficient of drag was found to increase of only 6-7% when installing trailing-edge inserts with fences.

I. Nomenclature

T	=	fences thickness (mm)
S	=	spacing between fences (mm)
H	=	height of the fences (mm)
R	=	fillet radius of the fences (mm)
c	=	chord length (m)
c_D	=	drag coefficient (-)
Re_c	=	Reynolds number based on the chord (-)
St_c	=	Strouhal number based on the chord (-)
δ_{99}	=	boundary-layer thickness (mm)
U_∞	=	free-stream velocity (ms^{-1})
U_e	=	edge velocity (ms^{-1})
u_τ	=	friction velocity (ms^{-1})

II. Introduction

In any flow adjacent to a solid surface, the layer of fluid in close proximity to the bounding surface forms a boundary layer. The broadband noise induced by the interaction of the boundary layer with the airfoil trailing-edge is known as trailing-edge noise. In aeroacoustics, the airframe noise is the aerodynamic noise generated by all the non-propulsive components of an aircraft. The airframe noise is the dominant contributor to the total noise emission of a landing aircraft [1]. Moreover, research shows that trailing-edge noise is among the main sources of airframe noise [2]. Trailing-edge noise is also the dominant aeroacoustic source of the wind turbines [3]. With the aim of attenuating the trailing-edge noise, several strategies were recently investigated, including trailing-edge brushes [4], trailing-edge serration [5, 6], porous materials [7, 8], jets injection [9], boundary layer blowing and suction [10, 11], and streamwise finlets [12]. These strategies were found to successfully attenuate the far-field noise. However, because they rely upon different physical mechanisms, their performance varies significantly both in terms of maximum achievable noise reduction as

*Marie-Curie Research Fellow, Delft University of Technology, AWEP Department, Kluyverweg 1, 2629 HS Delft, The Netherlands.
†PhD Researcher, Delft University of Technology, AWEP Department, Kluyverweg 1, 2629 HS Delft, The Netherlands.
‡Assistant Professor, Delft University of Technology, AWEP Department, Kluyverweg 1, 2629 HS Delft, The Netherlands.
§Professor, Delft University of Technology, AWEP Department, Kluyverweg 1, 2629 HS Delft, The Netherlands.

well as in the frequency range where that occurs.

Trailing-edge serration and porous materials can lead to a reduction of the far-field noise of as much as 8 dB at the low frequencies, i.e. in the interval $4 \leq St_c \leq 8$. However, research showed that the use of porous inserts at the trailing-edge of an airfoil deteriorates its aerodynamic performance. Adding a plate inside the insert appears to partially solve this problem, but it also negatively affects the aeroacoustics [13]. As a result, most of the noise reduction gained from using the porous inserts is lost when adding such solid plate. Trailing-edge serration is not associated with any significant penalties in the lifting performance of the airfoil. However, a drag increase of 10% or larger was reported [14]. Furthermore, deviations from zero angle of attack are accompanied by a progressively larger noise increase at high frequencies [14]. The described limitations associated with these techniques could be overcome when implementing active flow techniques. If conveniently tuned, uniform blowing and suction showed potentials to enhance the lift-to-drag ratio [15, 16] and to reduce the trailing-edge noise [10, 11]. Although early investigations on these active strategies of flow control appear promising, their implementation produces a considerable increase in their complexity, and therefore in their cost. Moreover, active techniques necessitate of a certain energy supply, which should be considered when assessing their performance. In this context, the use of streamwise finlets emerges as an interesting solution. Inspired by the downy canopy covering the surface of the external flight feathers of many owl species, these surface treatments were proposed by Clark *et al.* (2017) [12].

In their experimental wind tunnel measurements, Clark *et al.* (2017) investigated the effects of finlets on a tripped DU96-W180 airfoil at chord Reynolds numbers of up to 3 million. Streamwise finlets of two geometries were examined, i.e. fences and rails, with a particular focus on the effects of fences parameters encompassing height, spacing, thickness, and extension. The treatment provided up to 10 dB broadband reduction of trailing-edge noise, and it remained effective over an angle-of-attack interval extending over 9 degrees from zero degrees. The drag increase associated with the treatment was assessed using a drag rake, even though only for the configuration having the highest fences. Fences as high as 8 mm were found to produce a 10% increase of drag, which is almost entirely attributed to an increase in the wetted surface area. Even if the measurements showed that for decreasing spacing and for increasing height and thickness the aeroacoustics improve, it remains unclear what are their effects on the drag, and what is the physical mechanism for noise reduction. More recently, numerical simulations evidenced that two physical mechanisms for the noise reduction are at play [17, 18]. Firstly, the fences render the scattering process inefficient by increasing the distance between the source of noise, i.e. the turbulence structures, and the scattering edge. Secondly, the fences reduce the spanwise coherence in the boundary layer for separation distances larger than the fence spacing. The dominance of one mechanism over the others depends on the spacing between the fences.

The effects of streamwise fences on the turbulence properties of a turbulent boundary layer were also investigated experimentally [19]. Treatments with fences having a thickness of 0.5 mm, a height of 12 mm, and four values of the spacing, i.e. 1, 2, 4, 8, 12 mm, were connected to a flat plate through a half-a-millimeter substrate. Spectra of pressure fluctuations revealed different behaviours depending on whether the spacing is coarse or fine, with the transition between these occurring at a spacing of 4 mm. In particular, while reducing the spacing from 12 mm to 4 mm attenuates the energy content at the high frequencies, a further reduction of the spacing below 4 mm is not associated with any spectral attenuation. On the contrary, it produces an increase of the noise at the low frequencies, and so more when reducing the spacing from 4 mm to 1 mm. According to the authors, a spacing of the same order of magnitude as the inner layer of the turbulent boundary layer leads to an optimum in the reduction of the surface pressure fluctuations. Even though the ultimate goal of the study of Afshari *et al.* (2019) is to identify a configuration for the fences that minimizes the trailing-edge noise, the far-field noise was not measured directly. Therefore the attenuation of the surface pressure fluctuations could not be related with the far-field noise reduction.

Experimental analyses combining the direct measurement of the far-field noise and a detailed analysis into the flow turbulence were carried out on a NACA0012 airfoil [20]. The study shows that an optimum exists for the height of the fences leading to the largest noise reduction. This is of 0.6 times the boundary layer thickness, which also evidences a dependence of the optimal height on the angle of attack. The authors state that the streamwise position of the fences should not be precisely at the trailing-edge, but slightly upstream, specifically at 0.9 times the airfoil chord c. The results, however, do not exhibit any significant differences in the far-field noise reduction obtained for fences positioned at 0.9 c when compared to their positioning at the trailing-edge (at 1 c), as can be seen in their figure 6. Regarding to the spacing of the fences, it is concluded that the optimum is obtained for a spacing in the range between 4 mm and 6 mm, even though two cases solely were tested. A comprehensive analysis that systematically investigates the aeroacoustics and aerodynamics of an airfoil with fences finlets at different geometrical parameters is missing to date.

The present study is aimed at assessing *i.* how the different parameters for the fences finlets affect the far-field noise, *ii.* how they impact on the drag coefficient, *iii.* what is the dominant mechanism for noise reduction in relation

to the fences spacing. Specifically, the spacing between the fences is considered to have a significant effect on the mechanism of noise reduction as this is the parameter that mostly affects the flow behaviour according to the experiments of Afshari *et al.* (2019) [19]. In the first part of the study, the aspects described at the points *i.* and *ii.* are addressed experimentally, whereas an investigation into the physical mechanism for noise reduction with fences (point *iii.*) is performed numerically. In this paper, part of the experimental results are presented, whereas numerical simulations are currently running.

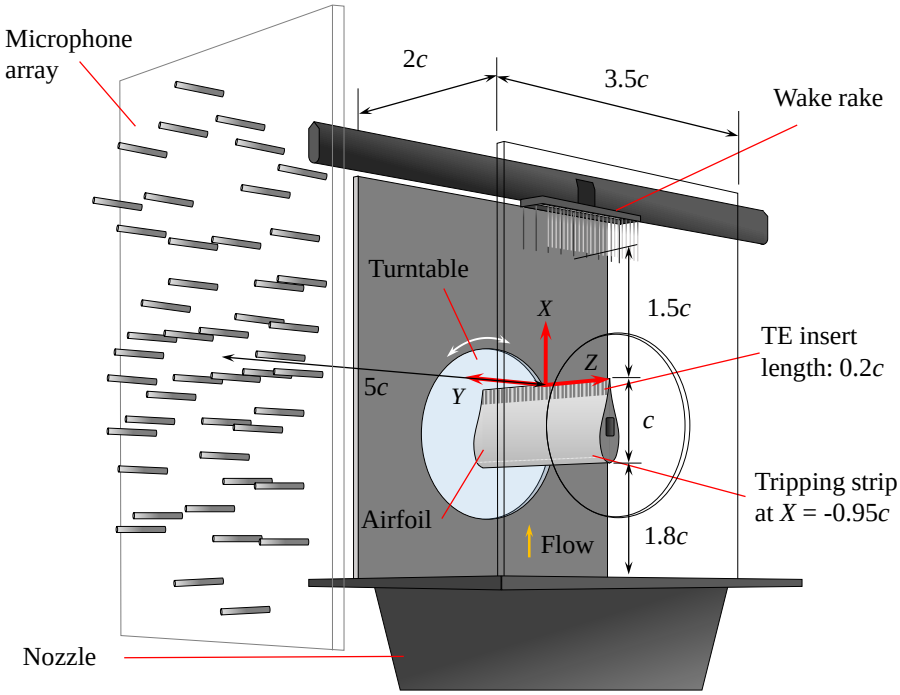

Fig. 1 Schematic of the wind-tunnel test set-up, measurement devices, and coordinate system.

III. Experimental methods

An airfoil model of a NACA633018 was used to test the passive technique of noise attenuation. Experimental investigations were performed in the anechoic vertical wind tunnel (A-Tunnel) at Delft University of Technology (TU Delft) [21]. The airfoil was mounted on a 400 mm × 700 mm nozzle opening via two parallel side plates. The chord c was 0.2 m and the span was two times the chord. The interchangeable TE inserts made up 20% of the chord. The same airfoil model was used in previous studies [22]. A schematic of the set-up is shown in Figure 1. Trailing-edge inserts carrying streamwise fences on both sides of the airfoil model were 3d-printed from a standard resin, where the nominal layer height was 50 μm. Having the fences directly on 3d-printed inserts avoided the use of a substrate to connect them to the airfoil surface, which had to be employed in all previous experimental studies. While the streamwise position of the fences as well as their shape were kept constant throughout the experimental campaign, their transversal spacing and height at the trailing-edge were varied from insert to insert. It is also worth highlighing that both transversal spacing and height were kept constant within each insert.

In figure 2, a CAD drawing of a trailing-edge insert is presented. The figure also shows the different geometrical parameters involved in the design of the surface treatment. Nine inserts carrying fences of different geometries were experimentally investigated. The spacing S, the height H at the trailing-edge, and the fillet radius R were varied, whereas the thickness T was kept constant and equal to T = 0.5 mm on each insert. The geometric parameters of the fences under analysis are summarized in table 1. The fillet radius R was of 1.25 mm for fences height of 2.5 mm, whereas it was of 2.20 mm for fences height of 4 mm or larger. In order to control the transition to turbulence of the boundary layer, stripes of zigzag tape were positioned along the span of the airfoil model on both sides of the airfoil, at 5% of the chord. The width of the zigzag tape was of 6 mm, the thickness was of 0.5 mm, and the angle was of 70°.

Acoustic measurements were performed inside the anechoic wind-tunnel through an array of microphones. The

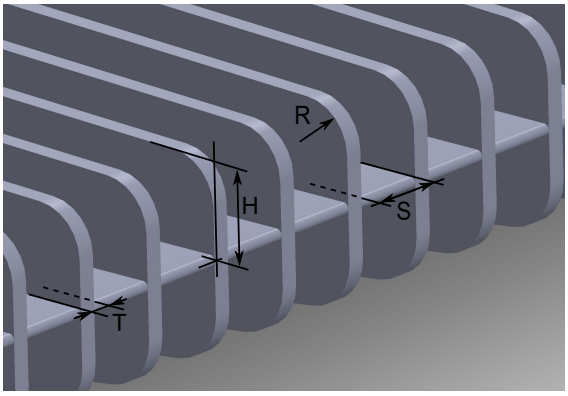

Fig. 2 CAD drawing of a trailing-edge insert used for its 3D-printing. The different geometrical parameters involved in the design are shown.

	S2H2p5	*S4H2p5*	*S4H4*	*S4H6*	*S6H2p5*	*S6H4*	*S6H6*	*S8H4*	*S8H6*
Spacing (mm)	2.0	4.0	4.0	4.0	6.0	6.0	6.0	8.0	8.0
Height (mm)	2.5	2.5	4.0	6.0	2.5	4.0	6.0	4.0	6.0

Table 1 Height and spacing of the fences on each trailing-edge insert.

array is constituted of 64 GRAS 40PH microphones having a frequency response ±1 dB and working in a frequency range from 10 Hz to 20 kHz, and designed for a maximum output of 135 dB ref. 2×10^5 Pa. The array is arranged in an optimized multi-arm spiral configuration, with the array plane placed parallel to the X-Z plane. The coordinate of the central microphone was $(X, Y, Z) = (0.45c, 5c, 0)$. The sampling time per case was 20 seconds with a sampling frequency of 51.2 kHz. The Cross-Spectral Matrix (CSM) of the signal was obtained by averaging the CSMs constructed from snapshots of the time-domain signal, weighted by the Hanning weighing function. Each snapshot contained 5120 samples, yielding the final frequency resolution of 10 Hz. The $5c \times 5c$ scan plane was defined with a distance of 10 mm between adjacent scan grid points, centered at the origin of the coordinate system. Conventional Frequency-Domain Beamforming (CFDBF) was first applied to reconstruct the acoustic source map. Then, in order to accurately extract only the TBL-TE noise from the source map, the source power integration (SPI) method was applied where the region of integration (ROI) was defined by a red square in the source maps. The ROI covers only half of the span in order to avoid possible corner sources. The SPLs below -6 dB relative to the maximum SPL in the CFDBF source map at each frequency were rejected from the integration to prevent inclusion of side lobes. Having obtained the source power, the SPLs were calculated using the reference distance of 1 m.

A wake survey was performed using a traversing wake rake to measure momentum deficits and thus extract the

U_∞ (ms^{-1})	$\alpha_{\text{eff.}}$ (°)	Re_c (–)	δ_{99} (mm)	δ^* (mm)	θ (mm)	U_e (ms^{-1})	u_τ (ms^{-1})	Π (–)
15	0	2×10^5	9.2	2.23	1.33	14.2	0.52	1.7
20		3×10^5	9.1	2.40	1.36	18.8	0.62	2.3
30		4×10^5	8.9	2.54	1.37	28.1	0.81	3.0

Table 2 Boundary-layer properties measured at the trailing edge of the airfoil at $\alpha = 0°$ with tripping at 5% of the chord.

profile drag coefficients c_D of the NACA633018 airfoil model with different TE inserts. The wake rake consisted of 50 and 12 total and static pressure probes, respectively. The total pressure probes spanned a distance of $1.1c$. The probe spacing varied from 3 to 12 mm with smaller spacing in the middle of the rake. The static pressure probes were uniformly distributed with a spacing of 12 mm. Pressure data were acquired by *HoneyWell TruStability* differential pressure transducers. The nominal accuracy of the transducers was of 3 Pa, while the sampling frequency was of 2 kHz. The wake rake was positioned at X = $2c$ and traversed between Z = -0.15c and Z = 0.35c. The center of the wake rake was adjusted according to the geometrical angle of attack such that it was aligned with the trailing edge and the momentum-deficit region in the wake was well contained within the wake rake span.

Boundary layer profiles close to the trailing–edge region were measured to determine the flow properties which are used for scaling and comparison of acoustic spectra. The measurements were performed with a hot-wire probe conditioned with a constant–temperature circuit. A single–sensor miniature wire probe model 55P15 (boundary–layer type) from Dantec Dynamics was used. The sensitive wire is made of platinum–plated tungsten having a length of 1.25 mm and a diameter of 5 μm. The probe was positioned at $X = -0.02c$ and $Z = -0.3c$ and was traversed in the $-Y$ direction using a Zaber LRQXXXHL–DE51T3 traverse controller. The wire temperature control and the data acquisition were done via a TSI IFA–300 CTA module and a NI–9234 data acquisition card respectively. Data was collected in 71 different points in the $-Y$ direction, with more data points collected near the wall. Each acquisition was of 2 seconds at the sampling frequency of 51.2 kHz. Calibration was done using forth–order polynomial curve fitting of the output voltages, with data from 17 speed–voltage data points logarithmically spaced between the lowest and the highest free–stream flow speed. The reference speed was measured upstream of the airfoil, i.e. close to the nozzle lip, and the velocity information was taken from a pitot tube installed near the hot-wire probe. Having obtained the velocity profiles, the edge velocity U_e as well as other properties of the turbulent boundary layer, such as the displacement thickness δ^*, momentum thickness θ, and the boundary-layer thickness δ_{99}, were extracted using an iterative method that has been found to work robustly with various experimental and simulated turbulent boundary layers subjected to pressure gradient [23]. The properties of the turbulent boundary layer measured at the trailing edge of the airfoil at $\alpha = 0^\circ$ with tripping at 5% of the chord are presented in table 2.

IV. Results

The aeroacoustic performance of the fences is assessed from spectra of the pressure signals acquired by the microphone array, as explained in the previous section. From each of these spectra, the spectrum of the airfoil with the baseline trailing-edge is subtracted with the aim of showing the extent of the noise reduction and noise increase as a function of the frequency. The noise attenuation spectra at different free-stream velocities and at constant angle of attack of $\alpha = 0^\circ$ are presented in figure 3. The application of fences is effective in reducing the far-field noise, and both their spacing and their height have an impact on the noise reduction performance.

At U_∞ = 15 ms^{-1}, all inserts are beneficial in reducing the noise over the whole range of frequencies under analysis. The largest noise attenuation, of as much as 6 dB, is obtained in the high-frequencies range for the insert S2H2p5. However, a spacing of 2 mm produces a lower noise reduction at low frequencies when compared with larger values of spacing. It can be observed that a clear bifurcation exists in the aeroacoustic behaviour of the fences when increasing the transversal spacing from 2 mm to 4 mm. The observed bifurcation is consistent with the spectra of wall-pressure fluctuations presented by Afshari *et al.* (2019) [19]. For values of the spacing of 4 mm or larger, the noise reduction appears to be much less frequency dependent. As a general trend, increasing the spacing is accompanied by a deterioration of the noise reduction performance. On the other hand, fences at increasing height exhibit moderately better performance at low frequency, but slightly worse performance at high frequencies. Variations on the transversal spacing between the fences have a much stronger impact on the aeroacoustics than changing the height of the fences. This is in agreement with previous experimental observations [12, 19].

At increasing free-stream velocities, the noise reduction performance of the fences tends to gradually deteriorate. The insert S2H2p5 experiences a decrease of the maximum noise attenuation, while a penalty in terms of noise increase is paid at the low frequencies. The maximum noise reduction decreases from 6 dB at 15 ms^{-1} to 5 dB at 20 ms^{-1}, and it becomes of 4 dB and of 3 dB at free-stream velocities of 25 ms^{-1} and of 30 ms^{-1}, respectively. Inserts having a transversal spacing of 4 mm and larger undergo a simultaneous deterioration of their levels of noise reduction both at low and at high frequencies. At mid frequencies, namely in the interval $1 - 3$ kHz, the maximum noise attenuation remains of approximately 2 dB when considering fences spacing of 4 mm and larger. This is obtained when installing the insert S4H4. At intermediate frequencies, a subtle improvement of the noise reduction can be observed for the inserts having values of spacing of 6 mm and of 8 mm.

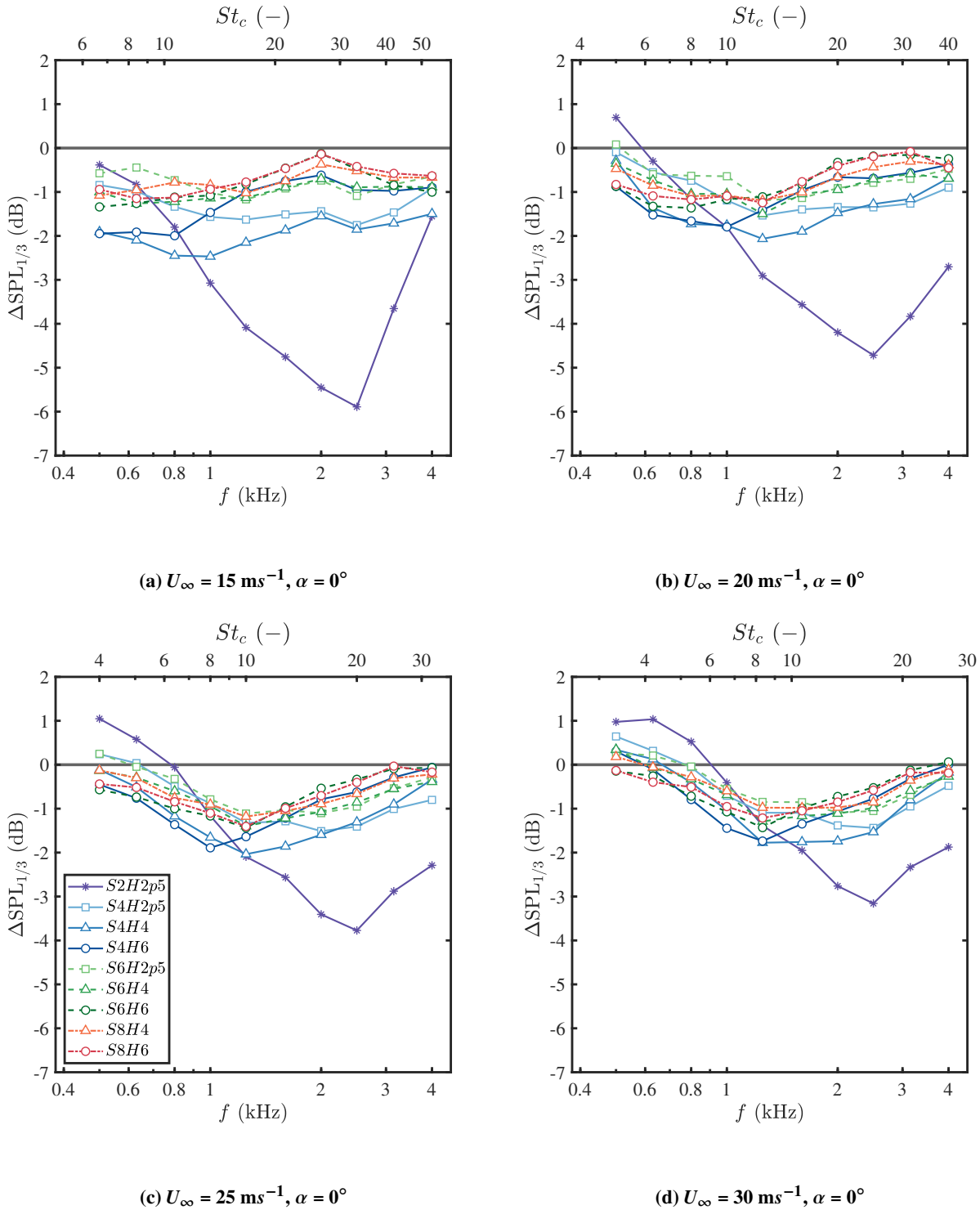

(a) U_∞ = 15 ms^{-1}, α = 0° **(b) U_∞ = 20 ms^{-1}, α = 0°**

(c) U_∞ = 25 ms^{-1}, α = 0° **(d) U_∞ = 30 ms^{-1}, α = 0°**

Fig. 3 Noise attenuation in 1/3-octave band as compared with the baseline configuration (black line), at four different values of free-stream velocity U_∞, and for a constant angle of attack of α = 0°.

The analysis of the spectra that was conducted thus far shows the aeroacoustic performance of the fences for an angle of attack equal to zero. To complement this investigation it would be of interest to also examine the effect of the

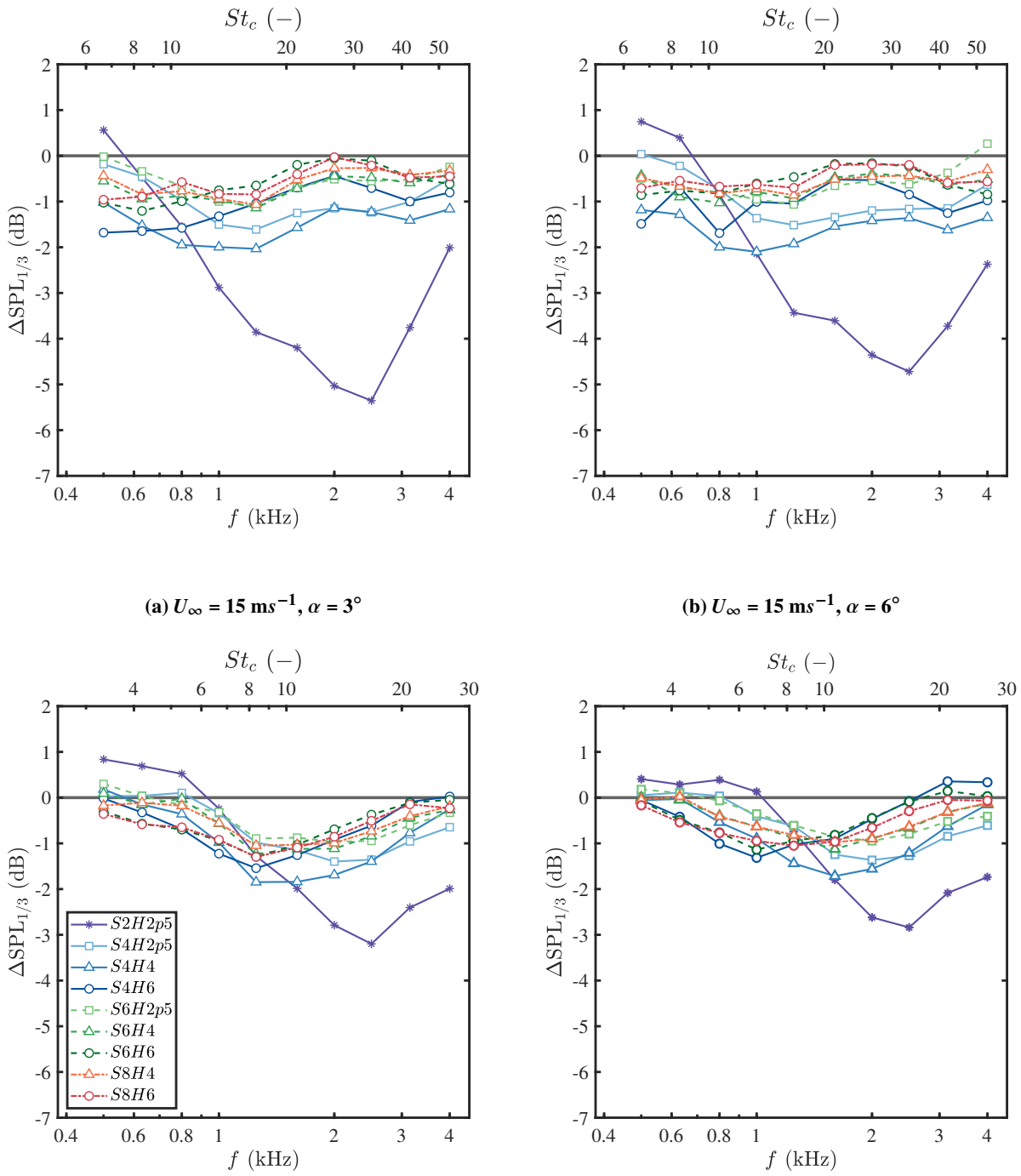

(a) U_∞ = 15 ms^{-1}, α = 3°

(b) U_∞ = 15 ms^{-1}, α = 6°

(c) U_∞ = 30 ms^{-1}, α = 3°

(d) U_∞ = 30 ms^{-1}, α = 6°

Fig. 4 Noise attenuation in 1/3-octave band as compared with the baseline configuration (black line), at four different values of free-stream velocity U_∞, and for a constant angle of attack of α = 0°.

angle of attack on the aeroacoustics. Spectra showing the levels of noise attenuation for geometric angles of attack of 3° and of 6° at the free-stream velocities of 15 ms^{-1} and 30 ms^{-1} are presented in figure 4. At U_∞ = 15 ms^{-1}, it appears

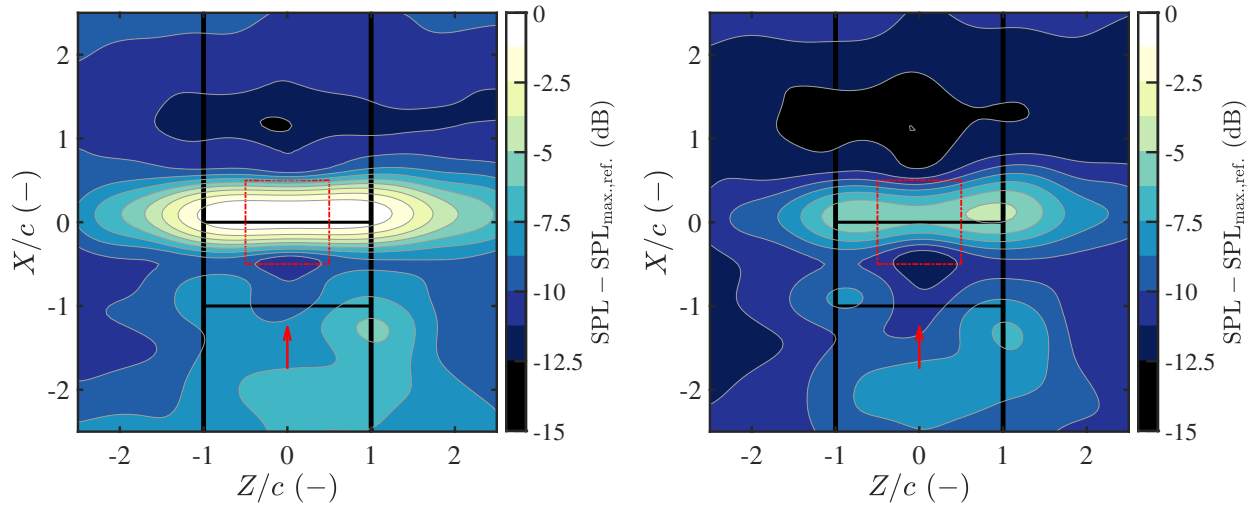

(a) Baseline, U_∞ = 20 ms^{-1}, α = 0°, $f_{1/3}$ = 2.5 kHz **(b) S2H2p5, U_∞ = 20 ms^{-1}, α = 0°, $f_{1/3}$ = 2.5 kHz**

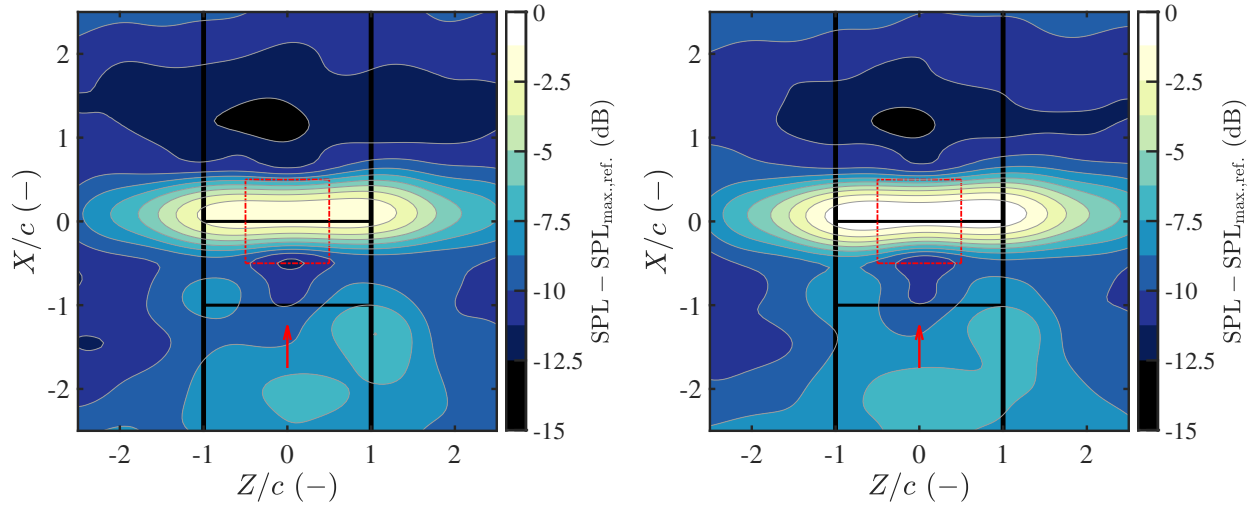

(c) S4H4, U_∞ = 20 ms^{-1}, α = 0°, $f_{1/3}$ = 2.5 kHz **(d) S6H6, U_∞ = 20 ms^{-1}, α = 0°, $f_{1/3}$ = 2.5 kHz**

Fig. 5 Noise source maps in 1/3-octave band at the frequency $f_{1/3}$ = 2.5 kHz as compared with the maximum of the baseline configuration, for three different trailing-edge inserts. The red square represents the region of integration, ROI, from which the spectra of SPL are obtained.

that increasing the angle of attack from 0° to 6° does not have any significant impact on noise reduction. For the insert S2H2p5, the maximum noise attenuation only diminishes by 1 dB, while at the low frequencies a modest penalty is paid in terms of noise increase. The family of inserts having the coarse spacing of 4 mm or larger is nearly insensitive to the described increase of the geometric angle of attack. At U_∞ = 30 ms^{-1}, increasing the angle of attack from 0° to 6° produces modest variations of the aeroacoustics. The maximum noise reduction that is obtained from the insert S2H2p5 remains unaffected by these changes of the angle of attack.

In figure 5, noise source maps from the baseline trailing-edge insert and from the inserts S2H2p5, S4H4, and S6H6 are presented at the frequency of 2.5 kHz as compared with the maximum of the baseline configuration. The red square represents the region of integration, ROI, from which the spectra of SPL are obtained, as explained in section III. What can be noticed is that the main source of noise is at the trailing edge of the airfoil, whereas the leading edge does not appear to generate any noise. From figure 5, the insert S2H2p5 produces the largest noise attenuation at the frequency of 2.5 kHz as could be previously observed from figure 3. The source map, however, shows that in proximity to the

corners of the ROI there is a stronger contribution to the integral as compared to the intermediate point. This evidences that the short span of the model produces a mild underestimation of the noise reduction from the fences.

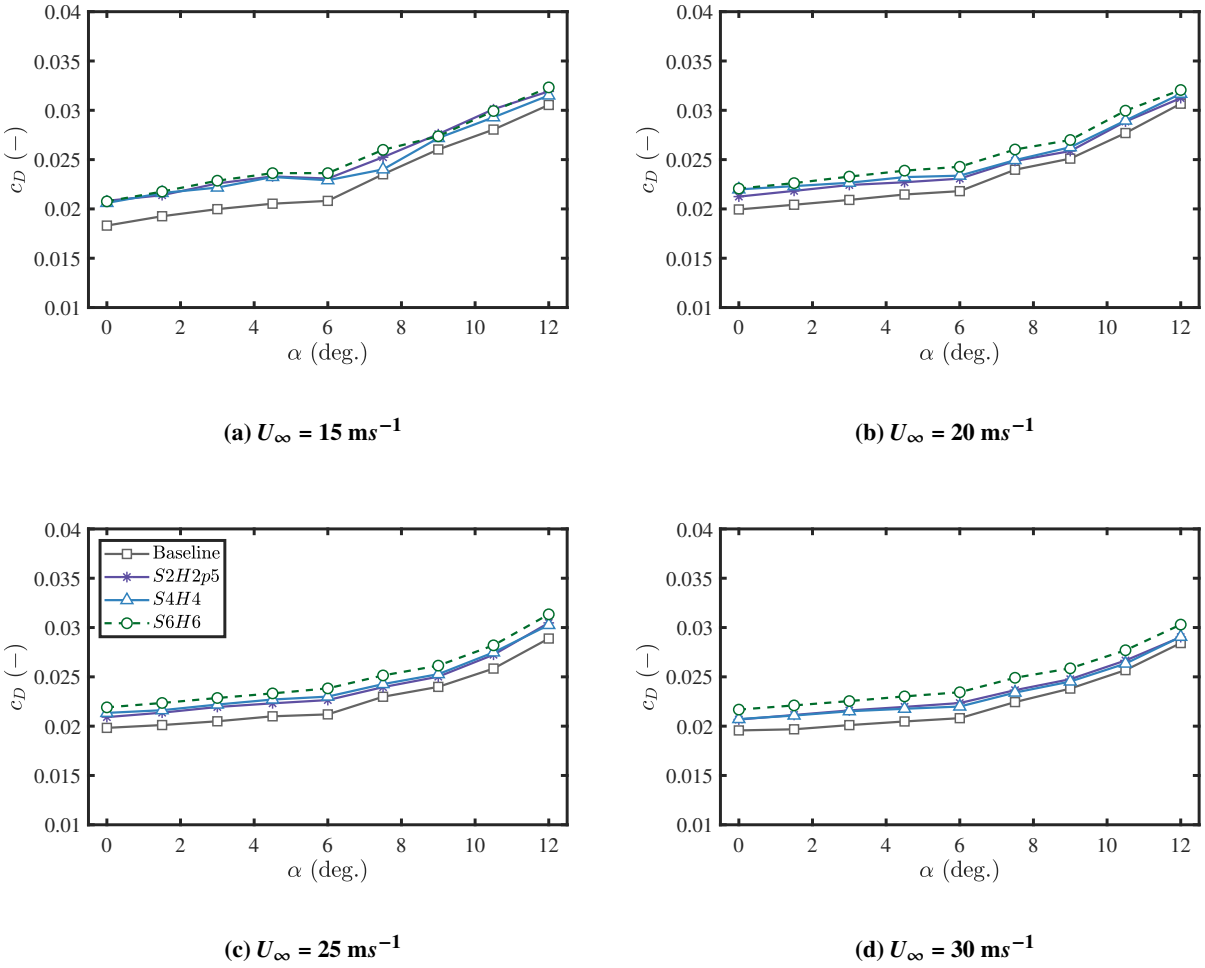

(a) U_∞ = 15 ms^{-1} **(b) U_∞ = 20 ms^{-1}**

(c) U_∞ = 25 ms^{-1} **(d) U_∞ = 30 ms^{-1}**

Fig. 6 Drag coefficients of the airfoil with different trailing-edge inserts as a function of the angle of attack, at four different free-stream velocities.

An estimate for the effect of the fences on the aerodynamics of the airfoil is necessary to have a complete characterization of these passive treatments. Measurements at different free-stream velocities and angles of attack were performed using a wake rake. The results of this assessment are presented in figure 6 for the baseline insert and for the inserts S2H2p5, S4H4, and S6H6. As a general observation, increasing the angle of attack produces a growth of the drag coefficient, and this trend becomes gradually stronger for decreasing the free-stream velocity. The difference in the coefficient of drag between the baseline insert and the inserts with fences becomes progressively smaller for increasing free-stream velocity. As expected, reducing the spacing between the fences as well as increasing their height leads to larger drag coefficients. However, while the aerodynamic performances of the inserts S2H2p5 and S4H4 are comparable, a sharp increase of drag is obtained for the insert S6H6, which leads to conclude that the effect of the fences height on drag is dominant. This evidence becomes progressively stronger for increasing free-stream velocity.

At U_∞ = 15 ms^{-1} and at an angle of attack of $\alpha = 0°$, a percentage difference of 14% exists between the baseline insert and the insert S2H2p5. When raising the free-stream velocity from U_∞ = 15 ms^{-1} to U_∞ = 20 ms^{-1}, the percentage difference between these drag coefficients reduces to 6.5%. Further growing the free-stream velocity does not produce any significant changes in the percentage difference between the baseline insert and the insert S2H2p5. At the free-stream velocity of U_∞ = 20 ms^{-1}, the percentage difference between the baseline insert and the insert S4H4 is

of 10%, but this percentage decreases to 6 % at $U_\infty = 30$ ms^{-1}, thus becoming similar to that of the insert S2H2p5. For angles of attack of $\alpha = 9^\circ$ or larger and at $U_\infty = 30$ ms^{-1}, the impact of the fences on the aerodynamics of the airfoil accounts for less than 5%.

V. Conclusion

Interchangeable trailing-edge inserts with streamwise fences of different spacing and height were installed on a NACA633018 as a strategy of noise reduction. Aeroacoustic measurements using an array of microphones were performed inside an anechoic wind tunnel. Fences having the finest spacing among the ones under investigation, i.e. a spacing of 2 mm, were found to produce the best noise reduction performance. A maximum noise reduction of 5-6 dB was achieved in the range of frequencies 1-3 kHz using the insert S2H2p5. Despite being the insert yielding the best aeroacoustic performance, this also produced the lowest increase of drag. For these reasons, further measurements assessing the aeroacoustic and aerodynamic behaviour of fences at low spacing will be carried out in the near future. Moreover, numerical simulations are currently running, which are aimed at investigating the physical mechanism for noise reduction of streamwise fences both at coarse and at fine spacing.

Acknowledgments

D.F. is funded by the Marie Skłodowska-Curie Actions of the European Union's Horizon 2020 Program under the Grant Agreement No. 895478 - ANACLETO.

References

[1] Casalino, D., Diozzi, F., Sannino, R., and Paonessa, A., "Aircraft noise reduction technologies: a bibliographic review," *Aerosp. Sci. Technol.*, Vol. 12, 2008, pp. 1–17.

[2] Brooks, T., Pope, D., and Marcolini, M., "Airfoil self-noise and prediction," *NASA Report No. 1218*, 1989.

[3] Oerlemans, S., Sijtsma, P., and Méndez López, B., "Location and quantification of noise sources on a wind turbine," *J. Sound Vib.*, Vol. 299, 2007, pp. 869–883.

[4] Herr, M., and Dobrzynski, W., "Experimental investigation in low-noise trailing-edge design," *AIAA J.*, Vol. 43, No. 6, 2005, pp. 1167–1175.

[5] Chong, T., Vathylakis, A., Joseph, P., and Gruber, M., "Self-noise produced by an airfoil with nonflat plate trailing-edge serrations," *AIAA J.*, Vol. 51, No. 11, 2013, pp. 65–77.

[6] Avallone, F., van der Velden, W. C. P., Ragni, D., and Casalino, D., "Noise reduction mechanisms of sawtooth and combed-sawtooth trailing-edge serrations," *J. Fluid Mech.*, Vol. 848, 2018, pp. 560–591.

[7] Showkat Ali, S. A., Azarpeyvand, M., and da Silva, C. R. I., "Trailing-edge flow and noise control using porous treatments," *J. Fluid Mech.*, Vol. 850, 2018, pp. 83–119.

[8] Rubio-Carpio, A., Merino-Martínez, R., Avallone, F., Ragni, D., Sneller, M., and van der Zwaag, S., "Experimental characterization of the turbulent boundary layer over a porous trailing edge for noise abatement," *J. Sound Vib.*, Vol. 443, 2019, pp. 537–558.

[9] Szőke, M., Fiscaletti, D., and Azarpeyvand, M., "Effect of inclined transverse jets on trailing-edge noise generation," *Phys. Fluids*, Vol. 30, No. 085110, 2018.

[10] Szőke, M., Fiscaletti, D., and Azarpeyvand, M., "Uniform flow injection into a turbulent boundary layer for trailing edge noise reduction," *Phys. Fluids*, Vol. 32, No. 085104, 2020.

[11] Szőke, M., Fiscaletti, D., and Azarpeyvand, M., "Influence of boundary layer flow suction on trailing edge noise generation," *J. Sound Vib.*, Vol. 475, No. 115276, 2020.

[12] Clark, I. A., Alexander, W. N., Devenport, W., Glegg, S., Jaworski, J. W., Daly, C., and Peake, N., "Bioinspired trailing-edge noise control," *AIAA J.*, Vol. 55, No. 3, 2017.

[13] Teruna, C., Menegar, F., Avallone, F., Ragni, D., Casalino, D., and Carolus, T., "Noise reduction mechanisms of an open-cell metal-foam trailing edge," *J. Fluid Mech.*, Vol. 898, No. A18, 2020.

[14] Gruber, M., "Airfoil noise reduction by edge treatments," Ph.D. thesis, University of Southampton, 2011.

[15] Kametani, Y., Fukagata, K., Örlü, R., and Schlatter, P., "Effect of uniform blowing/suction in a turbulent boundary layer at moderate Reynolds number," *Int. J. Heat Fluid Flow*, Vol. 55, 2015, pp. 132–142.

[16] Atzori, M., Vinuesa, R., Fahland, G., Stroh, A., Gatti, D., Frohnapfel, B., and Schlatter, P., "Aerodynamic effects of uniform blowing and suction on a NACA4412 airfoil," *Flow, Turbul. Combust.*, Vol. 105, 2020, pp. 735–759.

[17] Bodling, A., and Sharma, A., "Numerical investigation of low-noise airfoils inspired by the down coat of owls," *Bioinspir. Biomim.*, Vol. 14, No. 016013, 2019.

[18] Bodling, A., and Sharma, A., "Numerical investigation of noise reduction mechanisms in a bio-inspired airfoil," *J. Sound Vib.*, Vol. 453, 2019, pp. 314–327.

[19] Afshari, A., Azarpeyvand, M., Dehghan, A. A., Szőke, M., and Maryami, R., "Trailing-edge flow manipulation using streamwise finlets," *J. Fluid Mech.*, Vol. 870, 2019, pp. 617–650.

[20] Gstrein, F., Zang, B., and Azarpeyvand, M., "Application of finlets for trailing edge noise reduction of a NACA0012 airfoil," *AIAA Aviation Forum*, June 15-19, 2020.

[21] Merino-Martínez, R., Rubio Carpio, A., Pereira, L., van Herk, S., Avallone, F., Ragni, D., and Kotsonis, M., "Aeroacoustic design and characterization of the 3D-printed, open-jet, anechoic wind tunnel of Delft University of Technology," *App. Acoustics*, Vol. 170, 2020, p. 107504.

[22] Luesutthiviboon, S., Ragni, D., Avallone, F., and Sneller, M., "An alternative permeable topology design space for trailing-edge noise attenuation," *Int. J. Aeroacoust.*, Vol. 20, 2021, pp. 221–253.

[23] Kendall, A., and Koochesfahani, M., "A method for estimating wall friction in turbulent boundary layers," *AIAA Aviation Forum*, 2006.